Influence of Eu-substitution on Luminescent $CH_3NH_3PbBr_3$ Quantum Dots: Supporting Information

Lijia Liu, Jitao Li, and John A. McLeod*
Jiangsu Key Laboratory for Carbon-Based Functional Materials & Devices
Institute of Functional Nano and Soft Materials (FUNSOM)
Soochow University, Suzhou, Jiangsu, 215123 China
Joint International Research Laboratory of Carbon-Based Functional Materials and Devices
* E-mail: jmcleod@suda.edu.cn

April 22, 2018

Abstract

This supporting information contains details of fitting procedure for ultraviolet-visible (UV-vis) absorption spectra and photoluminescence (PL) emission spectra acquired from $MAPb_{1-x}Eu_xBr_3$ quantum dots (QDs). The fitted parameters for the UV-vis absorption spectra are tabulated in Tables S1-S7. The fitted parameters for the PL emission spectra are tabulated in Tables S8-S14. This supporting information also contains additional figures of: transmission electron microscopy (TEM) images with histograms of quantum dot sizes, shown in Figures S1-S7; measured UV-vis and PL spectra as a function of wavelength, shown in Figure S8; detailed fits of measured UV-vis spectra, shown in Figures S9-S15; and detailed fits of measured PL emission spectra, shown in Figures S16-S22.

1 Curve Fitting Procedures

All fits were performed using least-squares optimization, implemented using Scientific Python (SciPy). Uncertainties in the fitted variables were estimated using the Jacobian covariance matrix returned by the least-squares fitting function.

The UV-vis absorption spectra were fitted in energy space, first by removing any linear component in the onset (below 2.25 eV), then by fitting the Gaussian-broadened continuum joint density of states (JDOS):

$$j(\varepsilon) \quad = \quad A\int_{E_g}^{\infty} G(\varepsilon', \varepsilon, \sigma)\sqrt{\varepsilon' - E_g}d\varepsilon',$$

where $G(\varepsilon', \varepsilon, \sigma)$ is a Gaussian profile centred at ε with variance σ^2, A is a scaling amplitude, and E_g is the band gap. The variables A, σ, E_g are all fit such that the joint density of states is a close as possible to the measured spectrum without exceeding it at any point; in practice this is done by least-squares fitting that employs a modified residual, defined as:

$$\Delta(\varepsilon) \quad = \quad (y(\varepsilon) - j(\varepsilon)) + \frac{p}{2}\left[y(\varepsilon) - j(\varepsilon) - |y(\varepsilon) - j(\varepsilon)|\right],$$

where p is the "penalty factor" which forces fits where $j(\varepsilon) > y(\varepsilon)$ to be considered less optimal; here we used $p = 20$. Too large a penalty factor increases the importance of noise in the measured data when considering whether or not $j(\varepsilon) > y(\varepsilon)$, too small a penalty factor allows $j(\varepsilon) > y(\varepsilon)$ by a noticeable amount over a large energy range. We tested a variety of values for p before adopting $p = 20$ as an acceptable value for these data.

After obtaining the fitted joint density of states $j(\varepsilon)$, the UV-vis absorption spectra (the original data, with no prior treatment or background subtraction) were fit using a superposition of five Voigt functions, a linear background, and the scaled $j(\varepsilon)$:

$$y_{fit}(\varepsilon) = A_0 j(\varepsilon) + \sum_{i=1}^{5} A_i V(\varepsilon, \mu_i, \sigma_i, \gamma_i) + (m\varepsilon + b),$$

where $V(\varepsilon, \mu_i, \sigma_i, \gamma_i)$ is a Voigt profile (implemented using the real part of the Faddeeva function), where μ_i is the centre, σ_i^2 is the variance of the Gaussian profile, and $2\gamma_i$ the full-width at half-maximum of the Lorentz profile. Here all A_i, μ_i, σ_i, γ_i, slope m, and shift b are fitted using least-squares optimization.

Since visual examination of $y(\varepsilon) - j(\varepsilon)$ shows the residual has numerous Voigt-like peaks, determining a good initial guess for all parameters and the number of Voigt profiles to use in the fitting is relatively straight-forward.

The PL emission spectra were fitted in energy space using a superposition of Voigt profiles and a linear background:

$$y_{fit}(\varepsilon) = \sum_{i=1}^{N} A_i V(\varepsilon, \mu_i, \sigma_i, \gamma_i) + (m\varepsilon + b),$$

using the same variable names used for the UV-vis fitting. Here we found $N = 2$ gave best results for $MAPbBr_3$, while $N = 5$ was used for $MAPb_{1-x}Eu_xBr_3$ with $0 < x \leq 0.2$. For $x = 0.25$ and $x = 0.3$ we found that strangely $N = 5$ overfit the data, and a better result (i.e. one without Voigt profiles with excessively large widths, or those centred far outside the range of the measured PL spectrum) was obtained with $N = 4$. The fitted linear backgrounds from the PL emission spectra were very flat and close to zero, as expected.

2 Parameters from Curve Fitting

Component	A	μ (eV)	σ (eV)	γ (eV)
JDOS	1.09 ± 0.05	2.479 ± 0.005	0.10 ± 0.01	
Voigt 1	0.006 ± 0.001	2.404 ± 0.004	0.04 ± 0.009	0.03 ± 0.02
Voigt 2	0.011 ± 0.004	2.552 ± 0.002	0.01 ± 0.05	0.06 ± 0.02
Voigt 3	0.0062 ± 0.0005	2.6477 ± 0.0004	0.0239 ± 0.0008	0.0 ± 0.0008
Voigt 4	0.023 ± 0.004	2.7649 ± 0.0003	0.022 ± 0.003	0.023 ± 0.007
Voigt 5	0.04 ± 0.02	3.036 ± 0.002	0.05 ± 0.02	0.05 ± 0.04

Table S1: Fitted parameters for the UV-vis absorption spectrum of $MAPbBr_3$ QDs. For the JDOS, the centre μ is the band gap E_g. A linear background was also fit, obtaining a slope of $m = (0.094 \pm 0.005)$ eV^{-1} and a shift of $b = -0.135 \pm 0.007$.

Component	A	μ (eV)	σ (eV)	γ (eV)
JDOS	1.12 ± 0.04	2.461 ± 0.005	0.12 ± 0.01	
Voigt 1	0.007 ± 0.002	2.410 ± 0.003	0.032 ± 0.007	0.03 ± 0.01
Voigt 2	0.006 ± 0.005	2.519 ± 0.006	0.04 ± 0.03	0.04 ± 0.07
Voigt 3	0.0018 ± 0.0003	2.6466 ± 0.0007	0.019 ± 0.001	0.0 ± 0.003
Voigt 4	0.017 ± 0.003	2.7692 ± 0.0003	0.029 ± 0.003	0.011 ± 0.009
Voigt 5	0.02 ± 0.01	3.046 ± 0.004	0.05 ± 0.03	0.03 ± 0.06

Table S2: Fitted parameters for the UV-vis absorption spectrum of $MAPb_{1-x}Eu_xBr_3$ QDs for $x = 0.05$. For the JDOS, the centre μ is the band gap E_g. A linear background was also fit, obtaining a slope of $m = 0.117 \pm 0.004$ eV^{-1} and a shift of $b = -0.162 \pm 0.007$.

Component	A	μ (eV)	σ (eV)	γ (eV)
JDOS	1.13 ± 0.04	2.424 ± 0.004	0.092 ± 0.005	
Voigt 1	0.009 ± 0.003	2.396 ± 0.002	0.0 ± 0.3	0.06 ± 0.01
Voigt 2	0.016 ± 0.009	2.52 ± 0.01	0 ± 5	0.14 ± 0.04
Voigt 3	0.0027 ± 0.0002	2.6411 ± 0.0005	0.0208 ± 0.0009	0.0 ± 0.001
Voigt 4	0.020 ± 0.002	2.7600 ± 0.0002	0.025 ± 0.002	0.018 ± 0.006
Voigt 5	0.04 ± 0.02	3.042 ± 0.003	0.05 ± 0.02	0.07 ± 0.05

Table S3: Fitted parameters for the UV-vis absorption spectrum of $MAPb_{1-x}Eu_xBr_3$ QDs for $x = 0.1$. For the JDOS, the centre μ is the band gap E_g. A linear background was also fit, obtaining a slope of $m = 0.193 \pm 0.006$ eV^{-1} and a shift of $b = -0.27 \pm 0.01$.

Component	A	μ (eV)	σ (eV)	γ (eV)
JDOS	1.01 ± 0.04	2.411 ± 0.002	0.073 ± 0.006	
Voigt 1	0.009 ± 0.001	2.38 ± 0.01	0.107 ± 0.007	0.0 ± 0.002
Voigt 2	0.0027 ± 0.0008	2.5463 ± 0.0008	0.017 ± 0.005	0.01 ± 0.01
Voigt 3	0.015 ± 0.002	2.6315 ± 0.0003	0.023 ± 0.002	0.013 ± 0.004
Voigt 4	0.023 ± 0.003	2.7579 ± 0.0002	0.021 ± 0.002	0.023 ± 0.005
Voigt 5	0.033 ± 0.009	3.007 ± 0.003	0.10 ± 0.01	0.0 ± 0.01

Table S4: Fitted parameters for the UV-vis absorption spectrum of $MAPb_{1-x}Eu_xBr_3$ QDs for $x = 0.15$. For the JDOS, the centre μ is the band gap E_g. A linear background was also fit, obtaining a slope of $m = 0.210 \pm 0.003$ eV^{-1} and a shift of $b = -0.291 \pm 0.005$.

Component	A	μ (eV)	σ (eV)	γ (eV)
JDOS	1.05 ± 0.04	2.478 ± 0.004	0.10 ± 0.01	
Voigt 1	0.008 ± 0.003	2.414 ± 0.004	0.04 ± 0.02	0.05 ± 0.04
Voigt 2	0.001 ± 0.001	2.548 ± 0.004	0.01 ± 0.03	0.02 ± 0.04
Voigt 3	0.0023 ± 0.0007	2.636 ± 0.001	0.019 ± 0.003	0.0 ± 0.006
Voigt 4	0.044 ± 0.003	2.7689 ± 0.0002	0.031 ± 0.001	0.003 ± 0.004
Voigt 5	0.05 ± 0.04	3.12 ± 0.09	0.07 ± 0.07	0.06 ± 0.07

Table S5: Fitted parameters for the UV-vis absorption spectrum of $MAPb_{1-x}Eu_xBr_3$ QDs for $x = 0.2$. For the JDOS, the centre μ is the band gap E_g. A linear background was also fit, obtaining a slope of $m = 0.172 \pm 0.007$ eV^{-1} and a shift of $b = -0.24 \pm 0.01$.

Component	A	μ (eV)	σ (eV)	γ (eV)
JDOS	1.05 ± 0.04	2.491 ± 0.002	0.074 ± 0.004	
Voigt 1	0.012 ± 0.002	2.415 ± 0.003	0.0 ± 0.2	0.09 ± 0.02
Voigt 2	0.0006 ± 0.0007	2.556 ± 0.003	0 ± 2	0.02 ± 0.03
Voigt 3	0.0059 ± 0.0006	2.6424 ± 0.0004	0.025 ± 0.001	0.0 ± 0.001
Voigt 4	0.034 ± 0.003	2.7701 ± 0.0002	0.026 ± 0.001	0.016 ± 0.004
Voigt 5	0.03 ± 0.02	3.050 ± 0.007	0.06 ± 0.02	0.06 ± 0.04

Table S6: Fitted parameters for the UV-vis absorption spectrum of $MAPb_{1-x}Eu_xBr_3$ QDs for $x = 0.25$. For the JDOS, the centre μ is the band gap E_g. A linear background was also fit, obtaining a slope of $m = 0.123 \pm 0.004$ eV^{-1} and a shift of $b = -0.172 \pm 0.008$.

Component	A	μ (eV)	σ (eV)	γ (eV)
JDOS	1.111 ± 0.004	2.4841 ± 0.0005	0.052 ± 0.001	
Voigt 1	0.021 ± 0.001	2.3927 ± 0.0005	0.050 ± 0.004	0.048 ± 0.007
Voigt 2	0.0129 ± 0.0005	2.6344 ± 0.0001	0.0258 ± 0.0008	0.004 ± 0.002
Voigt 3	0.0127 ± 0.0003	2.7406 ± 0.0002	0.0288 ± 0.0005	0.0 ± 0.001
Voigt 4	0.0035 ± 0.0003	2.8635 ± 0.0005	0.025 ± 0.001	0.0 ± 0.003
Voigt 5	0.011 ± 0.001	2.994 ± 0.001	0.074 ± 0.003	0.0 ± 0.001

Table S7: Fitted parameters for the UV-vis absorption spectrum of $MAPb_{1-x}Eu_xBr_3$ QDs for $x = 0.3$. For the JDOS, the centre μ is the band gap E_g. A linear background was also fit, obtaining a slope of $m = 0.150 \pm 0.003$ eV^{-1} and a shift of $b = -0.229 \pm 0.006$.

Component	A	μ (eV)	σ (eV)	γ (eV)
Voigt 1	600 ± 200	2.37373 ± 0.00005	0.026 ± 0.002	0.019 ± 0.008
Voigt 2	600 ± 200	2.3733 ± 0.0001	0.059 ± 0.005	0.010 ± 0.009

Table S8: Fitted parameters for the PL emission spectrum of $MAPbBr_3$ QDs. A linear background was also fit, obtaining a slope of $m = -10 \pm 2$ eV^{-1} and a shift of $b = 15 \pm 6$.

Component	A	μ (eV)	σ (eV)	γ (eV)
Voigt 1	2600 ± 300	2.3638 ± 0.0001	0.0265 ± 0.0009	0.026 ± 0.003
Voigt 2	3400 ± 300	2.390 ± 0.001	0.062 ± 0.001	0.015 ± 0.002
Voigt 3	250 ± 40	2.557 ± 0.003	0.060 ± 0.008	0.0 ± 0.02
Voigt 4	90 ± 10	2.708 ± 0.001	0.02 ± 0.01	0.019 ± 0.002
Voigt 5	31 ± 5	2.833 ± 0.003	0.03 ± 0.01	0.01 ± 0.01

Table S9: Fitted parameters for the PL emission spectrum of $MAPb_{1-x}Eu_xBr_3$ QDs for $x = 0.05$. A linear background was also fit, obtaining a slope of $m = -15 \pm 2$ eV^{-1} and a shift of $b = -70 \pm 10$.

Component	A	μ (eV)	σ (eV)	γ (eV)
Voigt 1	2400 ± 200	2.3628 ± 0.0001	0.0262 ± 0.0009	0.029 ± 0.003
Voigt 2	3300 ± 200	2.390 ± 0.001	0.0598 ± 0.0009	0.014 ± 0.003
Voigt 3	160 ± 20	2.585 ± 0.004	0.072 ± 0.007	0.0 ± 0.01
Voigt 4	300 ± 20	2.7108 ± 0.0004	0.012 ± 0.003	0.034 ± 0.003
Voigt 5	102 ± 6	2.8265 ± 0.0004	0.028 ± 0.001	0.002 ± 0.003

Table S10: Fitted parameters for the PL emission spectrum of $MAPb_{1-x}Eu_xBr_3$ QDs for $x = 0.1$. A linear background was also fit, obtaining a slope of $m = -12 \pm 7$ eV^{-1} and a shift of $b = -90 \pm 20$.

Component	A	μ (eV)	σ (eV)	γ (eV)
Voigt 1	2230 ± 20	2.3732 ± 0.0001	0.0382± 0.0001	0.0 ± 0.00002
Voigt 2	5480 ± 60	2.3906 ± 0.0001	0.0606 ± 0.0006	0.028 ± 0.001
Voigt 4	300 ± 100	2.7 ± 0.5	2.1 ± 0.5	0.04 ± 0.02
Voigt 3	280 ± 10	2.7042 ± 0.0004	0.0 ± 0.05	0.039 ± 0.001
Voigt 5	39 ± 5	2.8243 ± 0.0007	0.023 ± 0.003	0.0 ± 0.006

Table S11: Fitted parameters for the PL emission spectrum of $MAPb_{1-x}Eu_xBr_3$ QDs for $x = 0.15$. A linear background was also fit, obtaining a slope of $m = -10 \pm 10$ eV^{-1} and a shift of $b = -200 \pm 100$.

Component	A	μ (eV)	σ (eV)	γ (eV)
Voigt 1 1200 ± 100	2.3541 ± 0.0001	0.0320 ± 0.0007	0.0 ± 0.003	
Voigt 2 5500 ± 100	2.3713 ± 0.0004	0.0559 ± 0.0003	0.0220 ± 0.0002	
Voigt 3 50 ± 5	2.5040 ± 0.0005	0.022 ± 0.001	0.0 ± 0.003	
Voigt 4 109 ± 5	2.7092 ± 0.0006	0.040 ± 0.002	0.004 ± 0.004	
Voigt 5 128 ± 4	2.8176 ± 0.0003	0.026 ± 0.001	0.011 ± 0.002	

Table S12: Fitted parameters for the PL emission spectrum of $MAPb_{1-x}Eu_xBr_3$ QDs for $x = 0.2$. A linear background was also fit, obtaining a slope of $m = -33 \pm 5$ eV^{-1} and a shift of $b = -30 \pm 10$.

Component	A	μ (eV)	σ (eV)	γ (eV)
Voigt 1	500 ± 100	2.3702 ± 0.0002	0.036 ± 0.002	0.003 ± 0.009
Voigt 2	3300 ± 100	2.3967 ± 0.0009	0.0616 ± 0.0003	0.0203 ± 0.0006
Voigt 3	280 ± 10	2.747± 0.002	0.064 ± 0.003	0.0 ± 0.004
Voigt 4	440 ± 10	2.8230 ± 0.0001	0.0254 ± 0.0003	0.0086 ± 0.0009

Table S13: Fitted parameters for the PL emission spectrum of $MAPb_{1-x}Eu_xBr_3$ QDs for $x = 0.25$. A linear background was also fit, obtaining a slope of $m = -60 \pm 7$ eV^{-1} and a shift of $b = 70 \pm 20$.

Component	A	μ (eV)	σ (eV)	γ (eV)
Voigt 1	40 ± 50	2.368 ± 0.001	0.03 ± 0.01	0.0 ± 0.04
Voigt 2	730 ± 50	2.398 ± 0.002	0.0480 ± 0.0007	0.0300 ± 0.0008
Voigt 3	300 ± 10	2.752 ± 0.004	0.041 ± 0.004	0.050 ± 0.004
Voigt 4	300 ± 10	2.8189 ± 0.0001	0.0293 ± 0.0003	0.0 ± 0.001

Table S14: Fitted parameters for the PL emission spectrum of $MAPb_{1-x}Eu_xBr_3$ QDs for $x = 0.3$. A linear background was also fit, obtaining a slope of $m = -40 \pm 4$ eV^{-1} and a shift of $b = 44 \pm 8$.

3 Supplemental Figures

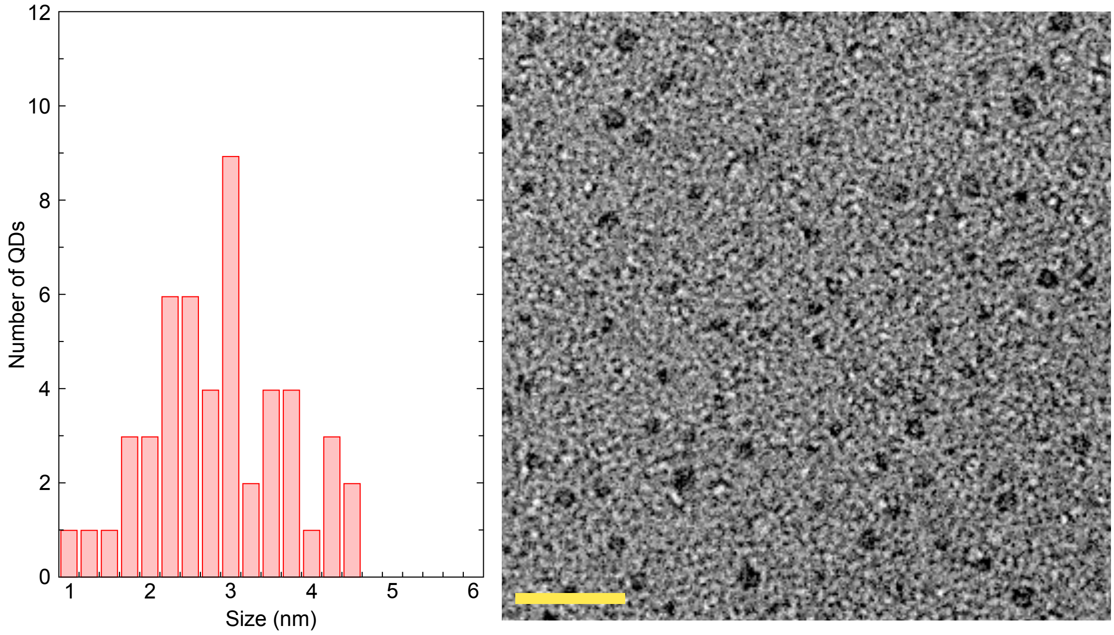

Figure S1: Histogram of QDs size (left), and TEM image (right) for $MAPbBr_3$ QDs. Scale bar is 20 nm.

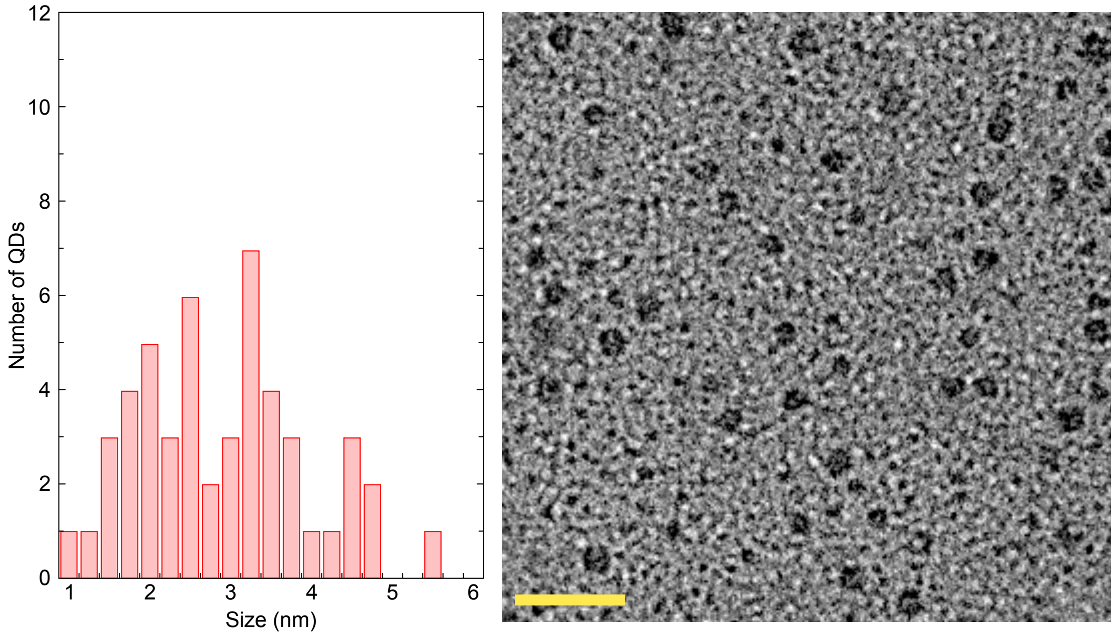

Figure S2: Histogram of QDs size (left), and TEM image (right) for $MAPb_{1-x}Eu_xBr_3$ QDs with $x = 0.05$. Scale bar is 20 nm.

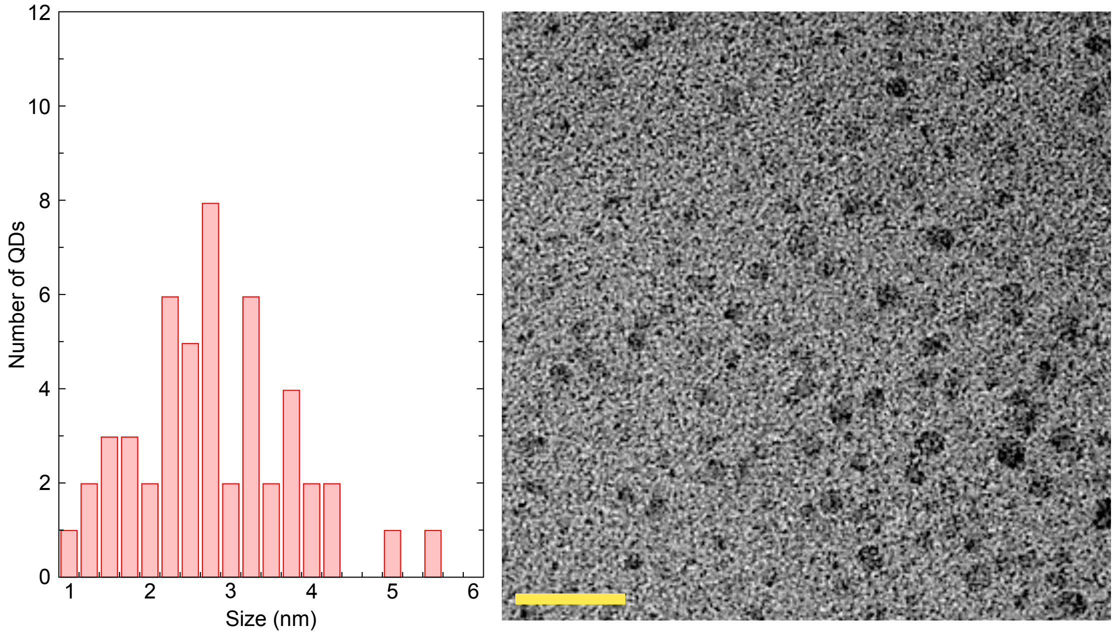

Figure S3: Histogram of QDs size (left), and TEM image (right) for $MAPb_{1-x}Eu_xBr_3$ QDs with $x = 0.1$. Scale bar is 20 nm.

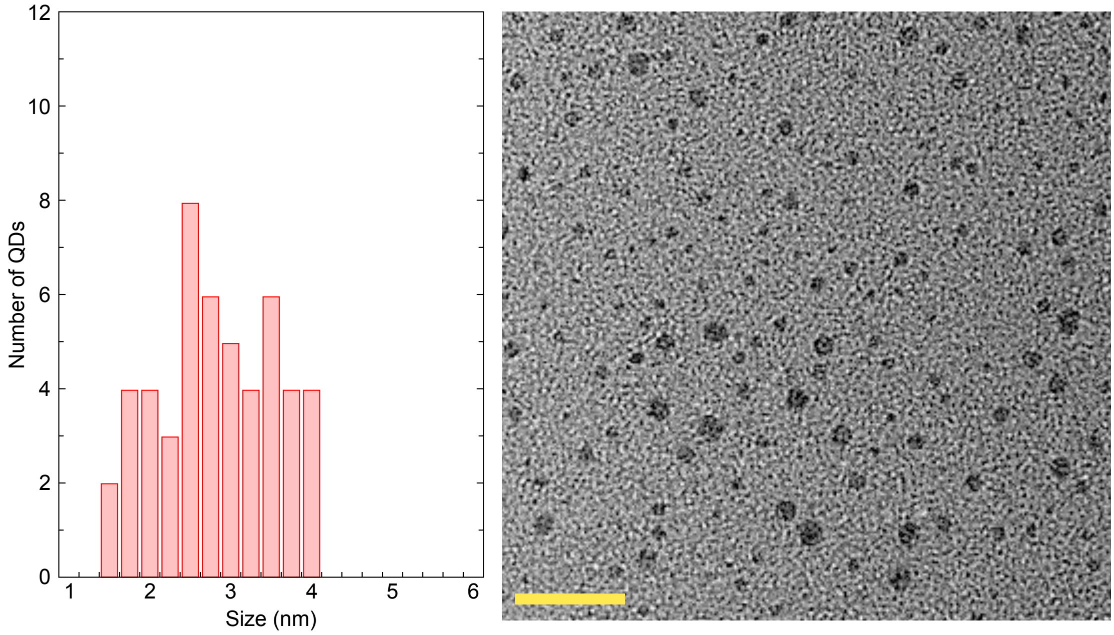

Figure S4: Histogram of QDs size (left), and TEM image (right) for $MAPb_{1-x}Eu_xBr_3$ QDs with $x = 0.15$. Scale bar is 20 nm.

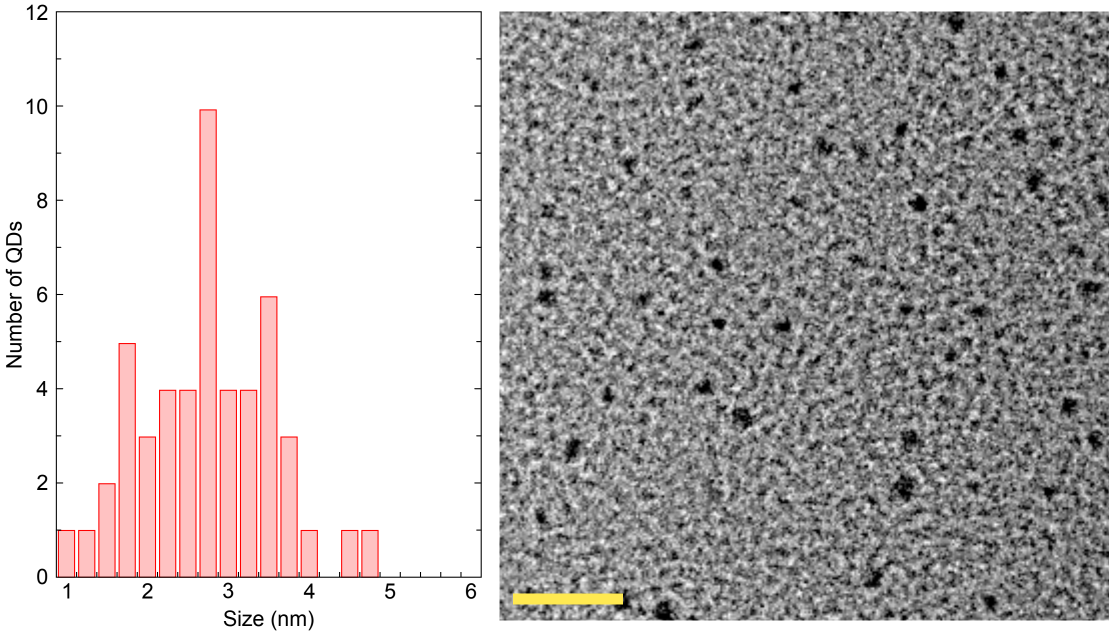

Figure S5: Histogram of QDs size (left), and TEM image (right) for $MAPb_{1-x}Eu_xBr_3$ QDs with $x = 0.2$. Scale bar is 20 nm.

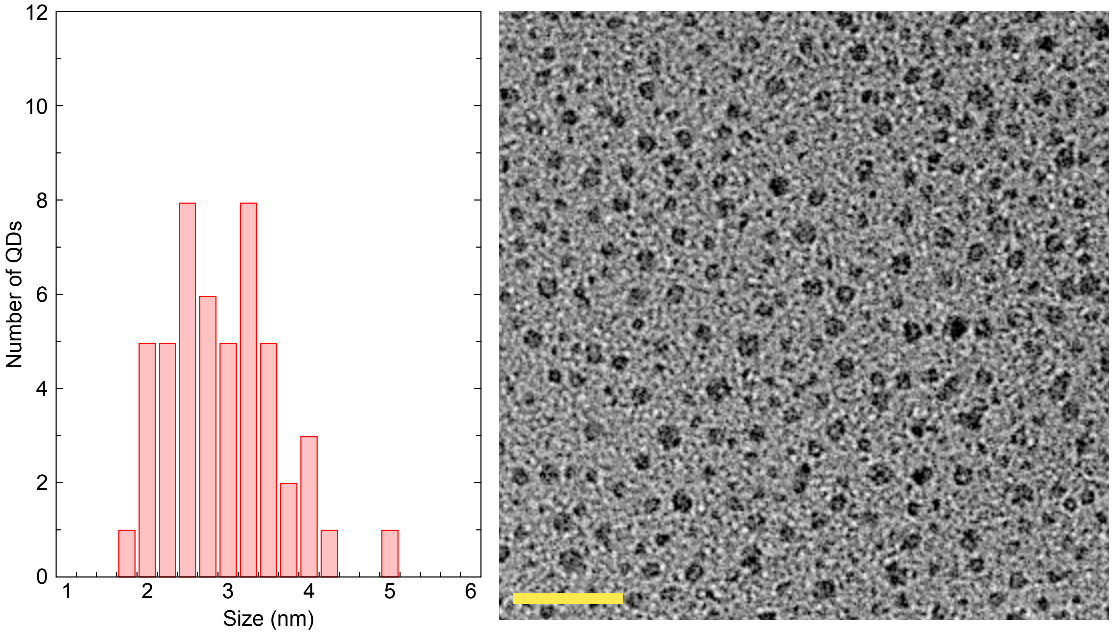

Figure S6: Histogram of QDs size (left), and TEM image (right) for $MAPb_{1-x}Eu_xBr_3$ QDs with $x = 0.25$. Scale bar is 20 nm.

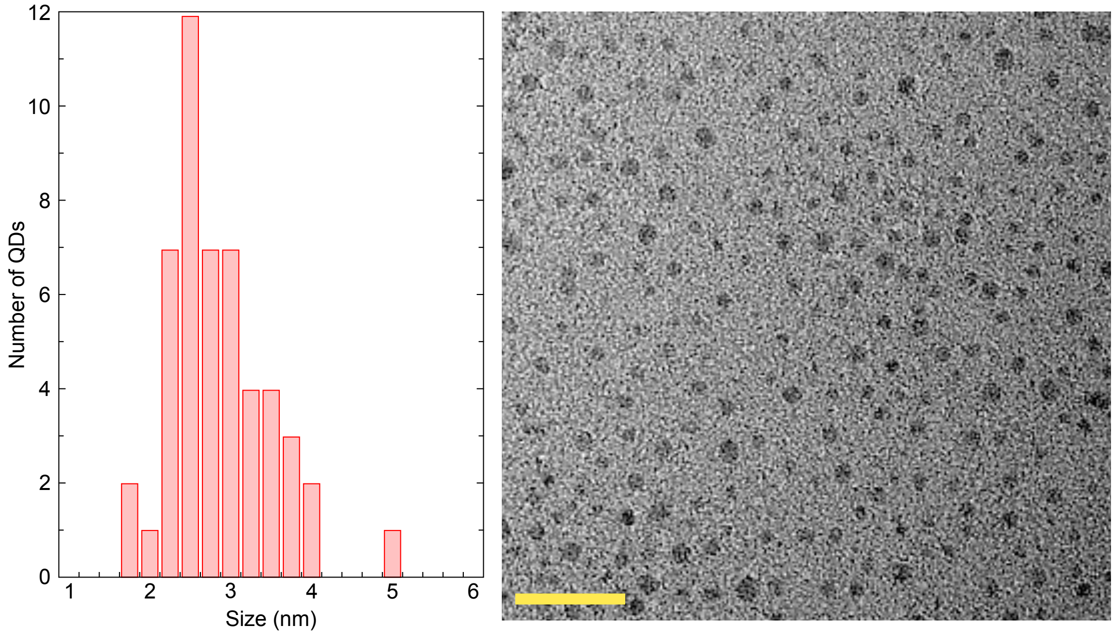

Figure S7: Histogram of QDs size (left), and TEM image (right) for $MAPb_{1-x}Eu_xBr_3$ QDs with $x = 0.3$. Scale bar is 20 nm.

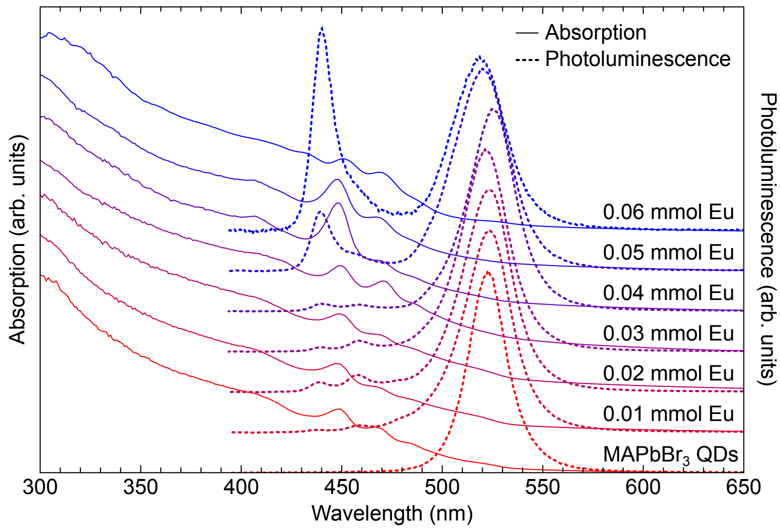

Figure S8: Measured UV-vis absorption and photoluminescence emission spectra for all QD solutions.

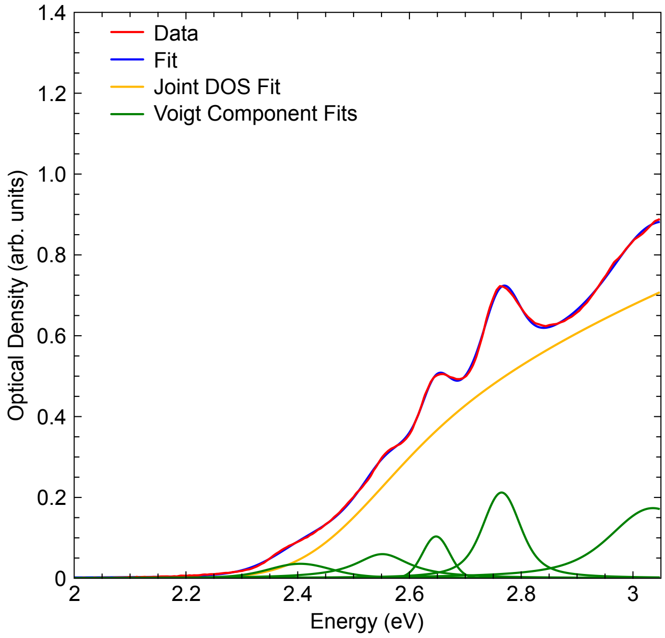

Figure S9: UV-vis spectrum fitting for $MAPbBr_3$ QDs.

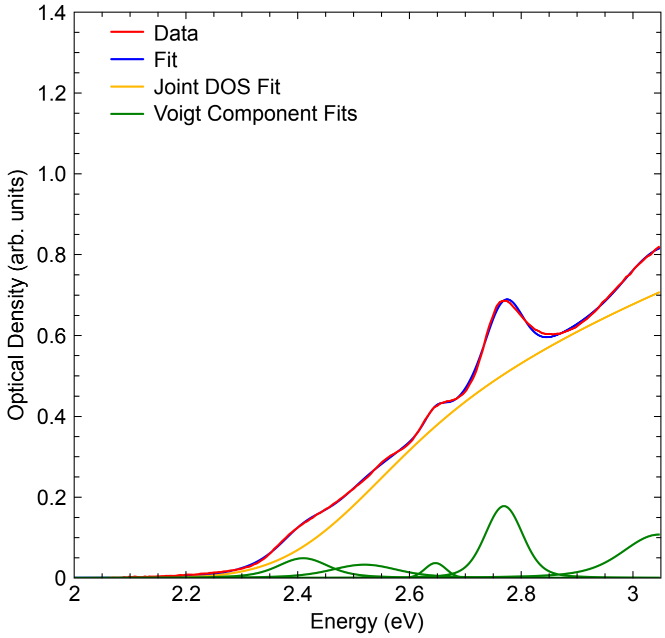

Figure S10: UV-vis spectrum fitting for $MAPb_{1-x}Eu_xBr_3$ QDs with $x = 0.05$.

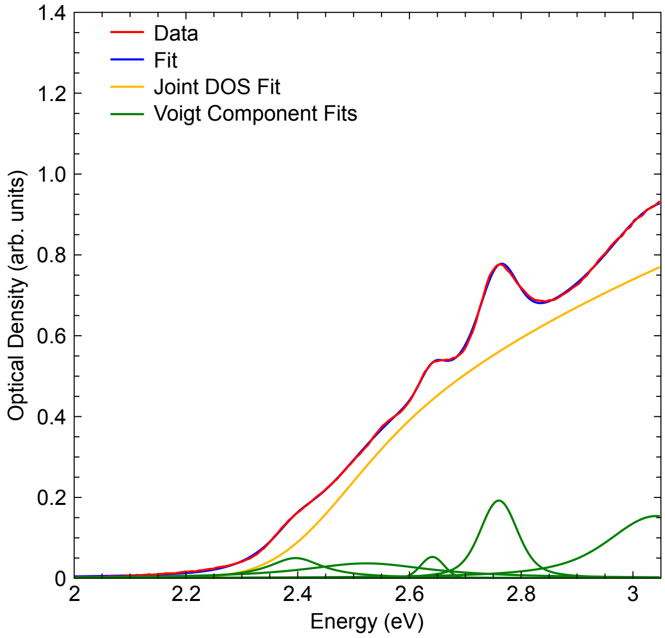

Figure S11: UV-vis spectrum fitting for $MAPb_{1-x}Eu_xBr_3$ QDs with $x = 0.1$.

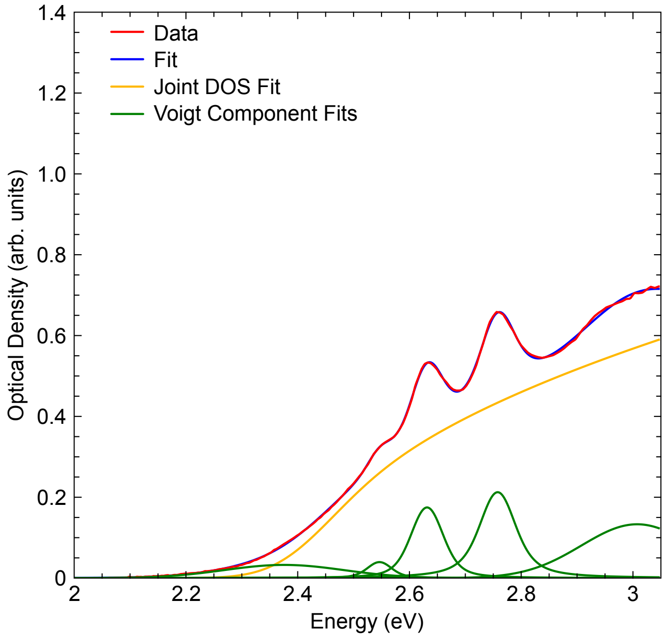

Figure S12: UV-vis spectrum fitting for $MAPb_{1-x}Eu_xBr_3$ QDs with $x = 0.15$.

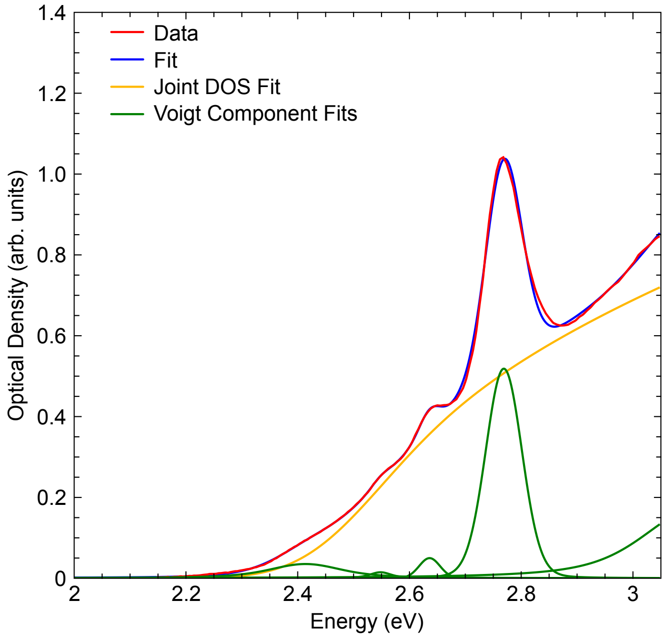

Figure S13: UV-vis spectrum fitting for $MAPb_{1-x}Eu_xBr_3$ QDs with $x = 0.2$.

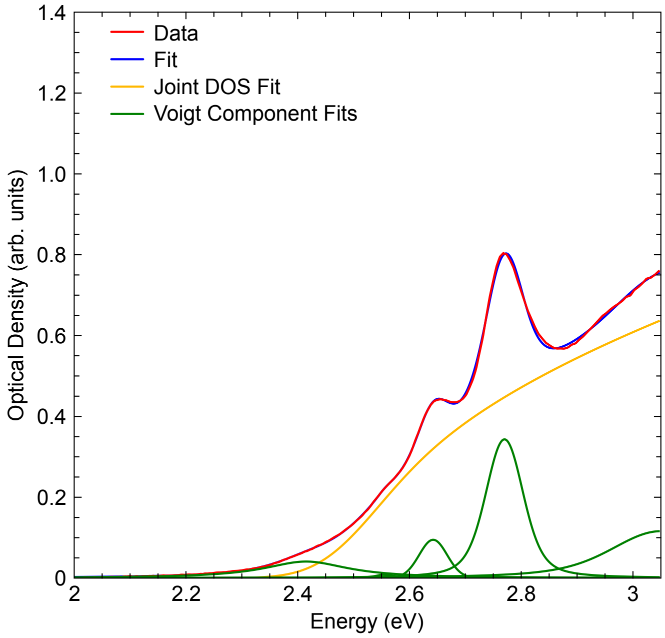

Figure S14: UV-vis spectrum fitting for $MAPb_{1-x}Eu_xBr_3$ QDs with $x = 0.25$.

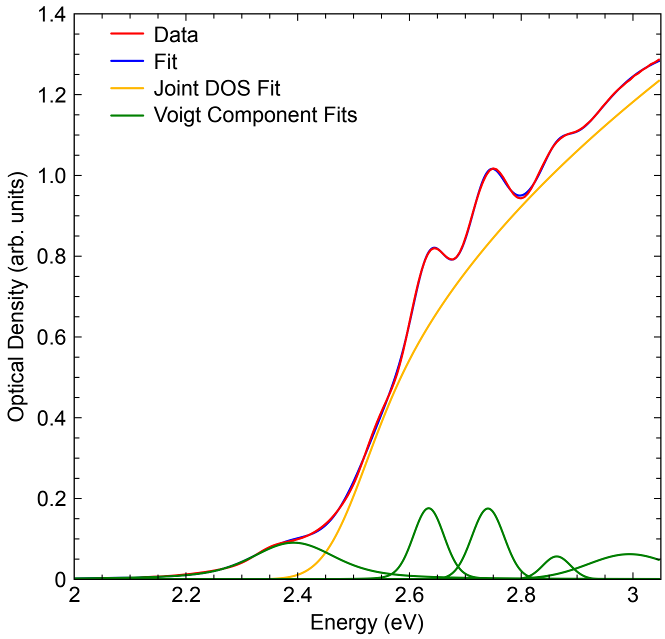

Figure S15: UV-vis spectrum fitting for $MAPb_{1-x}Eu_xBr_3$ QDs with $x = 0.3$.

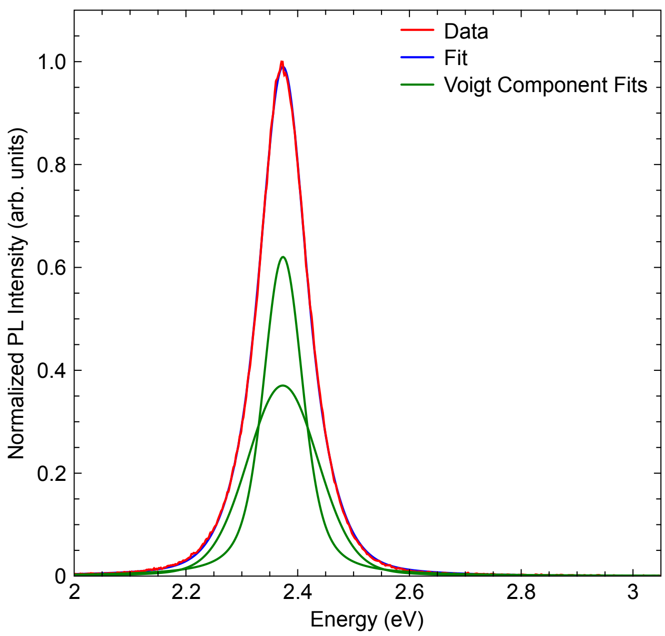

Figure S16: PL emission spectrum fitting for $MAPbBr_3$ QDs.

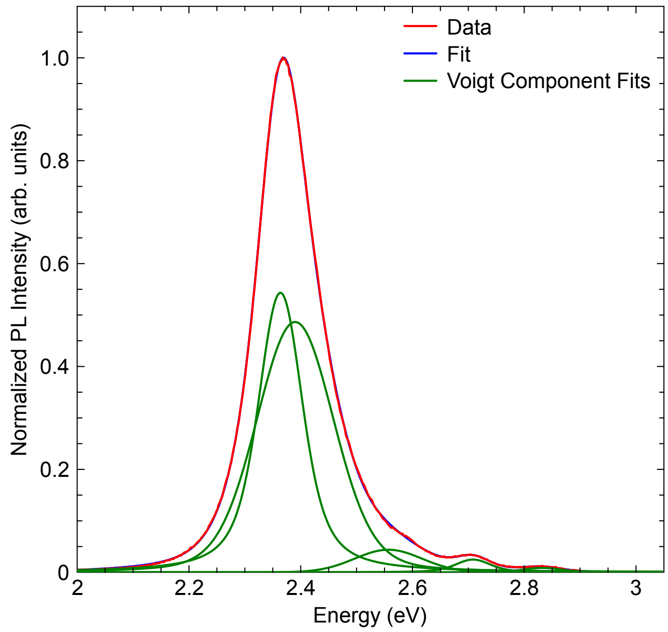

Figure S17: PL emission spectrum fitting for $MAPb_{1-x}Eu_xBr_3$ QDs with $x = 0.05$.

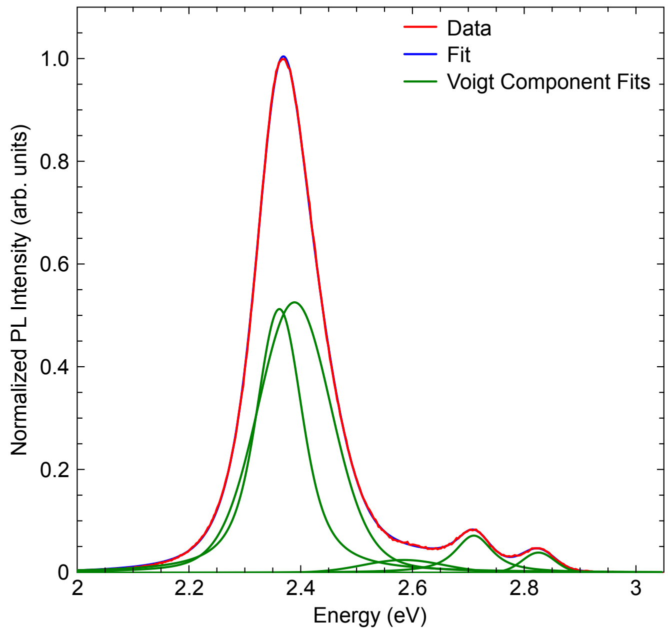

Figure S18: PL emission spectrum fitting for $MAPb_{1-x}Eu_xBr_3$ QDs with $x = 0.1$.

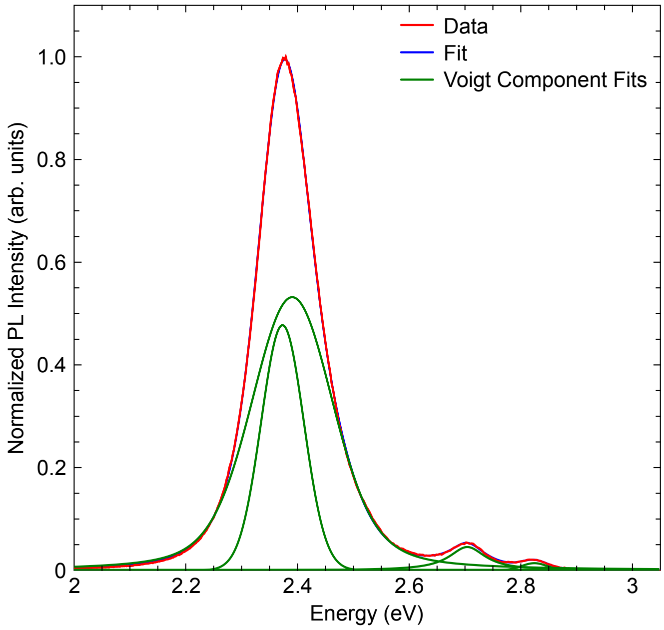

Figure S19: PL emission spectrum fitting for $MAPb_{1-x}Eu_xBr_3$ QDs with $x = 0.15$.

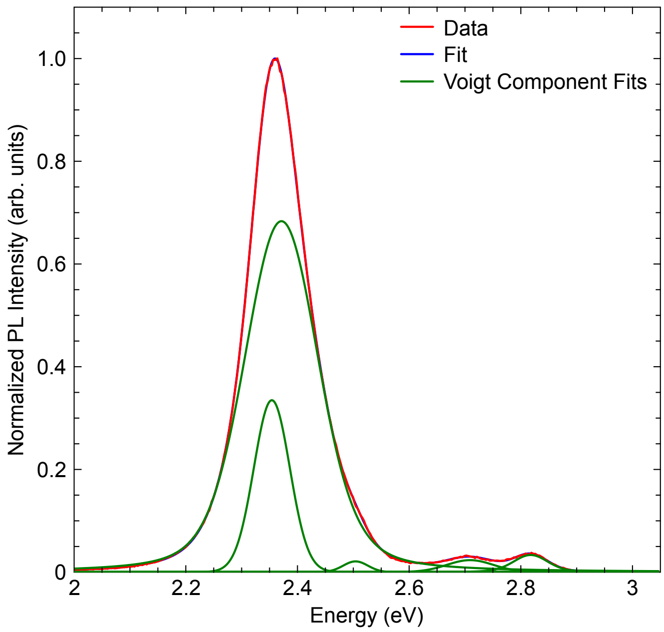

Figure S20: PL emission spectrum fitting for $MAPb_{1-x}Eu_xBr_3$ QDs with $x = 0.2$.

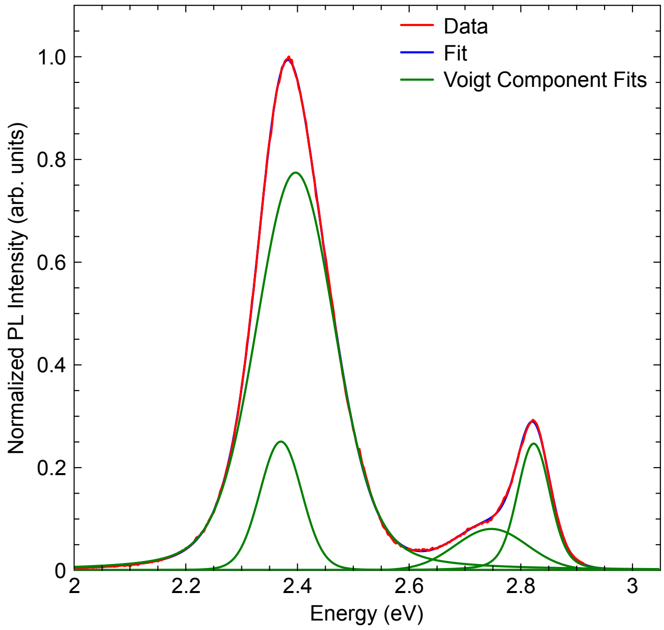

Figure S21: PL emission spectrum fitting for $MAPb_{1-x}Eu_xBr_3$ QDs with $x = 0.25$.

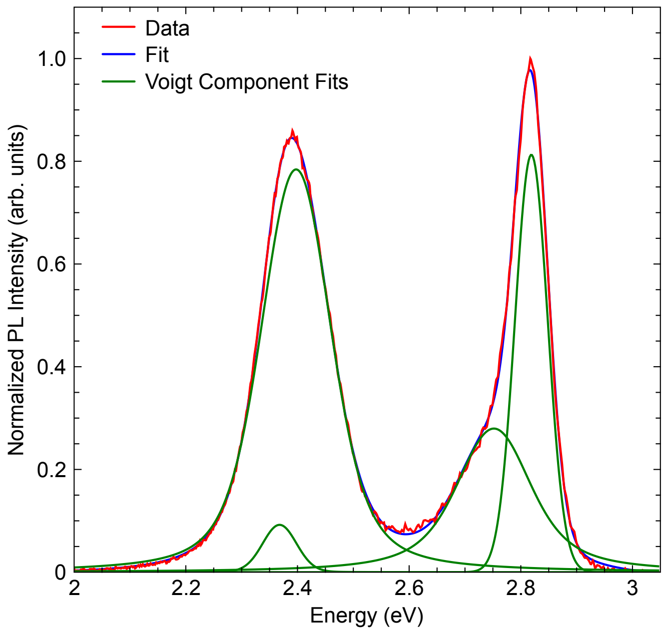

Figure S22: PL emission spectrum fitting for $MAPb_{1-x}Eu_xBr_3$ QDs with $x = 0.3$.